Draft version June 21, 2016
Preprint typeset using LaTeX style emulateapj v. 5/2/11

arXiv:1606.05955v1 [astro-ph.GA] 20 Jun 2016

GALAXY CANDIDATES AT $z \sim 10$ IN ARCHIVAL DATA FROM THE BRIGHTEST OF REIONIZING GALAXIES (BORG[z8]) SURVEY

S. R. Bernard[1,2], D. Carrasco[1], M. Trenti[1], P. A. Oesch[3,4], J. F. Wu[5], L. D. Bradley[6], K. B. Schmidt[7,8], R. J. Bouwens[9], V. Calvi[6], C. A. Mason[7,10], M. Stiavelli[6], T. Treu[10]

Draft version June 21, 2016

ABSTRACT

The Wide Field Camera 3 (WFC3) on the *Hubble Space Telescope* (*HST*) enabled the search for the first galaxies observed at $z \sim 8-11$ ($500-700$ Myr after the Big Bang). To continue quantifying the number density of the most luminous galaxies ($M_{AB} \sim -22.0$) at the earliest epoch observable with *HST*, we search for $z \sim 10$ galaxies (F125W-dropouts) in archival data from the Brightest of Reionizing Galaxies (BoRG[z8]) survey, originally designed for detection of $z \sim 8$ galaxies (F098M-dropouts). By focusing on the deepest 293 arcmin^2 of the data along 62 independent lines of sight, we identify six $z \sim 10$ candidates satisfying the color selection criteria, detected at S/N > 8 in F160W with $M_{\rm AB} = -22.8$ to -21.1 if at $z = 10$. Three of the six sources, including the two brightest, are in a single WFC3 pointing (~ 4 arcmin^2), suggestive of significant clustering, which is expected from bright galaxies at $z \sim 10$. However, the two brightest galaxies are too extended to be likely at $z \sim 10$, and one additional source is unresolved and possibly a brown dwarf. The remaining three candidates have $m_{AB} \sim 26$, and given the area and completeness of our search, our best estimate is a number density of sources that is marginally higher but consistent at 2σ with searches in legacy fields. Our study highlights that $z \sim 10$ searches can yield a small number of candidates, making tailored follow-ups of *HST* pure-parallel observations viable and effective.

Subject headings: cosmology: observations — galaxies: evolution — galaxies: formation — galaxies: high-redshift

1. INTRODUCTION

The epoch of reionization signified the appearance of the first stars and galaxies within the first billion years after the Big Bang, and the transformation of the intergalactic medium (IGM) from opaque to transparent. Despite recent progress, however, it is not yet fully understood. It is now well established that reionization is completed by $z \sim 6$ thanks to observations of the Lyα forest (e.g. Willott et al. 2007), and that the Universe was substantially ionized around redshift $z \sim 8$ when its age was less than 600 Myr, based on the electron scattering optical depth measured by Planck (Planck Collaboration et al. 2015). However, there is still substantial uncertainty regarding the sources of reionization. Can galaxies form with sufficient efficiency at such early times to provide enough reionizing photons (e.g. Alvarez, Finlator & Trenti 2012), or is the process possibly driven by other classes of objects such as AGN (Giallongo et al. 2012; Madau & Haardt 2015)?

Observationally, recent progress in near-IR detector technology has dramatically advanced our ability to search for galaxies during this epoch. Following the installation of the Wide Field Camera 3 (WFC3) on the *Hubble Space Telescope* (*HST*), a continuously growing sample of galaxy candidates at $z \gtrsim 7$ is accumulating thanks to a variety of surveys. These range from small-area ultradeep observations such as the Hubble Ultra-deep Field (HUDF, Illingworth et al. 2013), to shallower, larger-area searches for $L \gtrsim L_*$ galaxies either in legacy fields such as the Cosmic Assembly Near-infrared Deep Extragalactic Legacy Survey (CANDELS; Grogin et al. 2011; Koekemoer et al. 2011), or taking advantage of random-pointing opportunities like in the Brightest of Reionizing Galaxies (BoRG) survey (GO 11700, 12572, 13767; PI Trenti). Overall, a sample approaching 1000 galaxy candidates at $z > 7$ is known today (Bouwens et al. 2015a), and we are beginning to identify the first galaxy candidates from the first 500 million years ($z \sim 9-10$; Bouwens et al. 2011a, 2014, 2015a,b; Zheng et al. 2012; Coe et al. 2013; Ellis et al. 2013; McLure et al. 2013; Oesch et al. 2014; Zheng et al. 2014; Zitrin et al. 2014; McLeod et al. 2015; Ishigaki et al. 2015a; Infante et al. 2015).

These observations provide solid constraints on the galaxy luminosity function (LF) out to $z \sim 8$, which appears to be overall well described by a Schechter (1976) form, $\Phi(L) = \Phi^*(L/L^*)^\alpha \exp(-L/L^*)/L^*$, as at

[1] School of Physics, The University of Melbourne, Parkville, VIC 3010, Australia. Email: sbernard@student.unimelb.edu.au
[2] ARC Centre of Excellence for All-sky Astrophysics (CAASTRO).
[3] Yale Center for Astronomy and Astrophysics, Physics Department, New Haven, CT 06520, USA.
[4] Department of Astronomy, Yale University, New Haven, CT 06520, USA.
[5] Department of Physics and Astronomy, Rutgers, The State University of New Jersey, 136 Frelinghuysen Road, Piscataway, NJ 08854, USA
[6] Space Telescope Science Institute, 3700 San Martin Drive, Baltimore, MD 21218, USA.
[7] Department of Physics, University of California, Santa Barbara, CA 93106-9530, USA.
[8] Leibniz-Institut fur Astrophysik Potsdam (AIP), An der Sternwarte 16, 14482 Potsdam, Germany.
[9] Leiden Observatory, Leiden University, NL-2300 RA Leiden, The Netherlands.
[10] Department of Physics and Astronomy, UCLA, Los Angeles, CA, 90095-1547, USA.

lower redshift (Bouwens et al. 2007; Schmidt et al. 2014; Bouwens et al. 2015a; Finkelstein et al. 2015). However, other studies suggest that bright galaxy formation might not be suppressed as strongly at $z \gtrsim 7$, and either a single power law (Bouwens et al. 2011b; Finkelstein et al. 2015) or a double power law (Bowler et al. 2014) fit to the bright end of the LF has been explored. This change in the shape of the bright end is in turn connected theoretically to the physics of star formation in the most overdense and early forming environments where the brightest and rarest galaxies are expected to live (Muñoz & Loeb 2008; Trenti et al. 2012). A departure from a Schechter form could indicate a lower efficiency of feedback processes at early times, which in turn would imply an increase in the production of ionizing photons by galaxies. Additionally, at $z \geq 8$, the observed number density of bright galaxies is affected by magnification bias (Wyithe et al. 2011; Barone-Nugent et al. 2015a; Mason et al. 2015a; Fialkov & Loeb 2015), and this bias can cause the LF to take on a power-law shape at the bright end. Currently, the samples at $z \gtrsim 9$ are still too small to draw any conclusion on which scenario is realized, since only a handful of $z \sim 9-10$ candidates are known.

In addition to constraining the shape of the LF, the brightest high-z candidates identified by *HST* observations are also ideal targets for follow-up observations to infer stellar population properties such as ages and stellar masses (Stark et al. 2009; Labbé et al. 2010, 2015; Grazian et al. 2015), ionization state of the IGM (Muñoz & Loeb 2011), and spectroscopic redshift. For the latter, confirmation of photometric candidates relies typically on detection of a Lyman break in the galaxy continuum, (e.g., Malhotra et al. 2005) and/or of emission lines, primarily Lyman-α (e.g. Stark et al. 2010; Pentericci et al. 2011, 2014; Caruana et al. 2012; Schenker et al. 2012; Treu et al. 2012, 2013; Finkelstein et al. 2013; Tilvi et al. 2014; Vanzella et al. 2014) or other UV lines such as CIII] or CIV (Stark et al. 2015a,b). Spectroscopic follow-up for sources at $z \gtrsim 7.5$ is extremely challenging, with only limits on line emission resulting from most observations. Yet, the brightest targets show significant promise of detection based on the latest series of follow-ups which led to spectroscopic confirmation out to $z = 8.7$ (Zitrin et al. 2015), with several other Lyα detections at $z \gtrsim 7.5$ (Oesch et al. 2015; Roberts-Borsani et al. 2015).

With the goal of complementing the discovery of the rarest and most luminous sources in the epoch of reionization from legacy fields such as CANDELS, the Brightest of Reionizing Galaxies Survey (BoRG, see Trenti et al. 2011) has been carrying out pure-parallel, random pointing observations with WFC3 since 2010. BoRG identified a large sample ($n = 38$) of $z \sim 8$ Y-band dropouts with $L \gtrsim L_*$ (Trenti et al. 2011, 2012; Bradley et al. 2012; Schmidt et al. 2014; see also McLure et al. 2013; Bouwens et al. 2015a). This represents a catalog of galaxies that is not affected by large scale structure bias (sample or "cosmic" variance; see Trenti & Stiavelli 2008), which is especially severe for rare sources sitting in massive dark matter halos ($M_h \gtrsim 10^{11}$ M$_\odot$), as inferred from clustering measurements at $z > 7$ (Barone-Nugent et al. 2014). Follow-up spectroscopy of the BoRG dropouts with Keck and VLT has provided evidence for an increase of the IGM neutrality at $z \sim 8$ compared to $z \sim 6-7$ (Treu et al. 2012, 2013; Barone-Nugent et al. 2015b). Currently, a new campaign of observations is ongoing, with a revised filter-set optimized for the new frontier of redshift detection at $z \sim 9-10$ (BoRG[z9-10]; GO 13767, PI Trenti). Initial results from $\sim 25\%$ of the dataset (~ 130 arcmin^2) led to the identification of two candidates at $z \sim 10$ (Calvi et al. 2015) with $m_{\rm AB} \sim 25-25.5$, which are similar in luminosity to the spectroscopically confirmed $z = 8.7$ source reported by Zitrin et al. (2015), but significantly brighter than the six J-dropouts with $m_{\rm AB} \sim 26-27$ identified in the GOODS/CANDELS fields from a comparable area (Oesch et al. 2014).

These recent developments indicate that it might be possible for a small number of ultra-bright sources ($M_{\rm AB} \lesssim -22$) to be present as early as 500 Myr after the Big Bang. Thus, they prompted us to systematically analyze the BoRG archival data from observations in the previous cycles, which cover ~ 350 arcmin^2, to search for bright $z \sim 10$ candidates and constrain their number density. This paper presents the results of this search, and is organized as follows: Section 2 briefly introduces the BoRG dataset. Section 3 discusses our selection criteria for $z \sim 10$ sources (J_{125}-band dropouts), with results presented in Section 4. In Section 5, we determine the galaxy UV luminosity function at $z \sim 10$, and compare with previous determinations. Section 6 summarizes and concludes. Throughout the paper we use the Planck Collaboration et al. (2015) cosmology: $\Omega_\Lambda = 0.692$, $\Omega_M = 0.308$ and $H_0 = 67.8\,{\rm km\,s^{-1}\,Mpc^{-1}}$. All magnitudes are quoted in the AB system (Oke & Gunn 1983).

2. THE BORG SURVEY

We use data acquired as part of the Brightest of Reionizing Galaxies (BoRG[z8]) survey, which consists of core BoRG pointings (GO 11700, 12572, 12905), augmented by other pure parallel archival data (GO 11702, PI Yan, Yan et al. 2011) and COS GTO coordinated parallel observations. For an in-depth description of the survey, we refer the reader to Trenti et al. (2011); Bradley et al. (2012); Schmidt et al. (2014). Here, we use the 2014 (DR3) public release of the data[11], which consists of 71 independent pointings covering a total area of $\sim$350 arcmin^2. All fields were imaged using the WFC3/IR filters F098M, F125W and F160W, and in the optical V band, using either the WFC3 F606W or F600LP filter. We refer to the WFC3 F098M, F125W and F160W images as the Y_{098}, J_{125} and H_{160} images, and to the F606W and F600LP images as V_{606} and V_{600}, respectively.

Exposure times in each filter vary on a field-by-field basis, and 5σ limiting magnitudes for point sources and aperture $r = 0\farcs2$ are between $m_{\rm AB} = 25.6-27.4$, with a typical value of $m_{\rm AB} \sim 26.7$ (Trenti et al. 2011; Bradley et al. 2012; Schmidt et al. 2014). We note that since the dataset originates from parallel observations when the primary instrument is a spectrograph (COS or STIS), there is no dithering of the exposures. To compensate for the lack of dithering, the BoRG data reduction pipeline has been augmented with a customized Laplacian edge filtering algorithm developed by van Dokkum (2001). Overall, the lack of dithering has a minimal impact ($\Delta m < 0.1$) on the image and photometric quality,

[11] https://archive.stsci.edu/prepds/borg/

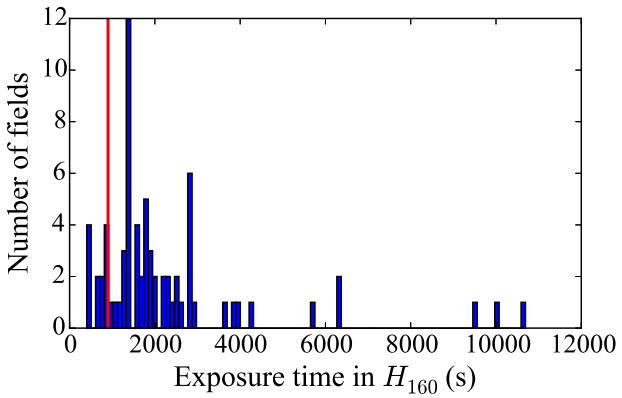

Figure 1. Histogram of the exposure time in H_{160} for the 71 BoRG[z8] fields. The vertical red line indicates $t_{\rm exp} = 900$ s. Fields with exposure times < 900 s in H_{160} were excluded from our analysis.

as it has been established through comparison between primary (dithered) versus pure-parallel observations of the same field (Calvi et al. 2015).

Since the BoRG[z8] survey was designed to have J_{125} as primary detection band, some fields have only a single short exposure in the H_{160}-band. To ensure a consistently high image quality, here we include in the analysis only those fields with total exposure time $t_{\rm exp} \geq 900$ s in H_{160}. This resulted in the exclusion of 9 fields out of 71, so that the area included in our study is 293 arcmin^2. The distribution of the exposure time in H_{160} for the fields in BoRG[z8] is shown in Figure 1.

The BoRG[z8] public data release consists of reduced and aligned science images produced with `MultiDrizzle` (Koekemoer et al. 2003) with a pixel scale of $0\farcs08$, as well as associated weight maps (see Bradley et al. 2012; Schmidt et al. 2014). Following our standard analysis pipeline to search for dropouts in the data (Trenti et al. 2011), we create RMS maps from the weight maps, and normalize them to account for correlated noise induced by `MultiDrizzle` (see Casertano et al. 2000). In short, this is done for each field and filter by measuring the noise in the image at random positions not associated with detected sources (i.e. the "sky" noise), and comparing the measurement with the value inferred from the RMS map, which can then be corrected by a multiplicative factor to match the measurement. Our rescaling factors are on average ~ 1.1 for the IR filters and ~ 1.4 for V (see also Trenti et al. 2011; Bradley et al. 2012; Schmidt et al. 2014). In addition, photometric zero-points are corrected to account for galactic reddening along each line of sight, according to Schlafly & Finkbeiner (2011).

Using `SExtractor` (Bertin & Arnouts 1996) in dual-image mode, we construct catalogues of sources in each field, using the H_{160}-band image for detection. Colors and signal to noise ratios are defined based on isophotal fluxes/magnitudes (FLUX_ISO), while we adopt MAG_AUTO for the total magnitude of each source.

3. SELECTION OF J_{125}-DROPOUTS

To select $z \sim 9-10$ galaxy candidates, we use the dropout technique (Steidel et al. 1996). At high z, neutral hydrogen in the IGM almost completely absorbs UV photons, leading to a break at the galaxy rest wavelength of Lyα (1216 Å). For galaxies between $z \sim 9-11$, this implies a drop in the J_{125}-filter, and non-detection in the V and Y_{098} bands.

Our focus on J_{125}-dropouts implies that our sample of candidates are essentially detected only in H_{160}. Therefore, to minimize the risk of introducing spurious sources, we require a clear detection in H_{160}, with $\mathrm{S/N}_H \geq 8$. We also impose a strong $J_{125} - H_{160}$ break, trading sample completeness for higher purity, and require a color cut: $J_{125} - H_{160} > 1.5$, which is more conservative than the typical $J_{125} - H_{160} > 1.2$ applied to legacy fields (e.g. Bouwens et al. 2015a) since we do not have the availability of multi-observatory data to constrain the continuum of candidates at longer wavelengths and help control contamination.

Overall, we impose the following criteria for selection as J_{125}-dropouts:

$$J_{125} - H_{160} > 1.5$$
$$\mathrm{S/N}_V < 1.5$$
$$\mathrm{S/N}_{098} < 1.5$$
$$\mathrm{S/N}_{160} \geq 8.0$$

When computing the $J_{125} - H_{160}$ color, if the J_{125}-band flux has $\mathrm{S/N} < 1$ we use the 1σ limit instead.

Finally, to reduce the risk of contamination from detector defects surviving the data reduction pipeline, we further impose a stellarity cut through the `SExtractor` CLASS_STAR parameter. We require CLASS_STAR < 0.95, where 1 corresponds to a point source, and 0 to a diffuse light profile. We then visually inspected the dropouts that meet these criteria to reject any remaining detector artifacts and diffraction spikes. All the sources that meet all criteria and pass the visual inspection are listed in Table 1, and discussed below.

4. RESULTS

We performed a search for J_{125}-dropouts over 293 arcmin^2 of archival BoRG data. We find six sources that satisfy the J_{125}-dropout selection with $\mathrm{S/N}_H \geq 8$. The candidates are detected over a range of magnitudes, with four candidates between $H_{160} = 25.8 - 26.4$, and two brighter candidates at $H_{160} = 24.7$ and $H_{160} = 25.2$. At $z = 10$, this corresponds to $\mathbf{M}_{\rm AB} = -21.1$ to -22.8. Three candidates are detected only in H_{160}, while the remaining three are detected in both J_{125} and H_{160}. The photometry of the candidates is reported in Table 1, and postage stamps of V, Y_{098}, J_{125}, and H_{160} are shown in Figure 2.

We derive photometric redshifts for these six candidates using the photo-z code BPZ (Benítez 2000), assuming a flat prior on redshift, motivated by the uncertainty in the density of sources at intermediate redshifts with colors similar to those of $z \gtrsim 9$ galaxies. For the single band (H_{160}) detections, the photometric redshift distribution is flat over the range $z \sim 10-13$. For the two-band (J_{125} and H_{160}) detections, the photometric redshifts are sharply peaked around $z = 10$. The photometric probability distributions are included in Figure 2 alongside the images of the candidates.

A comparison of the apparent H_{160} magnitude against the photometric redshift of our candidates against $z \geq 8$

Table 1
Photometry of J_{125}-dropouts

ID	RA (deg)	Decl. (deg)	H_{160}	$J_{125}-H_{160}$	S/N$_H$	S/N$_J$	S/N$_Y$	S/N$_V$	r_e	Stellarity	$M_{\rm AB}$[a]
borg_0240-1857_25	40.1195	-18.9726	26.24 ± 0.18	> 2.53	8.1	0.1	-0.1	1.0[b]	0.″13	0.71	−21.1
borg_0240-1857_129	40.1289	-18.9678	24.74 ± 0.07	2.21	14.5	2.5	0.6	0.9[b]	0.″33	0.02	−22.7
borg_0240-1857_369	40.1274	-18.9612	25.22 ± 0.11	1.88	9.6	2.2	-1.7	0.2[b]	0.″38	0.00	−22.3
borg_0456-2203_1091	73.9774	-22.0372	26.09 ± 0.13	> 2.47	8.1	-1.3	-0.4	0.1[c]	0.″24	0.51	−21.4
borg_1153+0056_514	178.1972	0.9270	26.31 ± 0.24	> 2.64	8.0	0.02	-0.1	-0.6[c]	0.″23	0.01	−21.2
borg_1459+7146_785	224.7239	71.7814	25.82 ± 0.14	1.57	12.8	3.7	-1.1	1.3[c]	0.″14	0.91	−21.5

[a] Assuming $z = 10$.
[b] V_{600}
[c] V_{606}

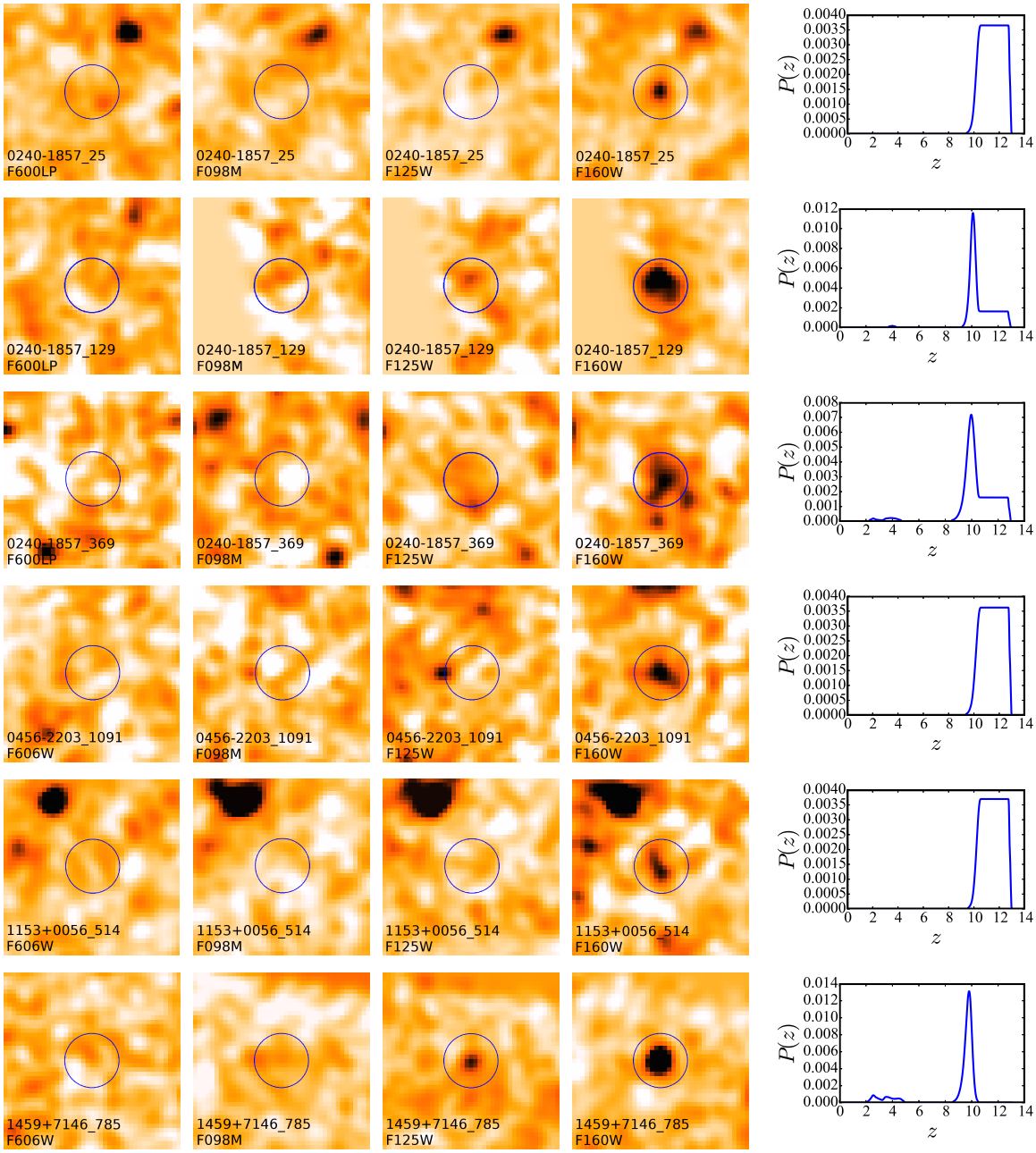

Figure 2. Postage stamps of the J_{125}-band dropouts listed in Table 1. Each image is $3.''2 \times 3.''2$. The diameter of each circle is $1.''0$. Each image and circle is centred on the candidate dropout galaxy. The left four columns show the candidate in V, Y_{098}, J_{125}, and H_{160}, while the right-most column shows the redshift probability distribution $P(z)$ vs z determined from BPZ for each candidate.

candidates from other *HST*/WFC3 surveys is shown in Figure 3. While two of our candidates are particularly bright in H_{160}, they are consistent with previously-discovered candidates at $z \sim 10$ by Calvi et al. (2015).

We also determine the size of the candidates, starting from the observed half-light (effective) radius as determined by `SExtractor`, which is translated into an intrinsic source size taking into account the effects of the point-spread function (PSF) broadening and surface brightness limits following Calvi et al. (2015). The empirical relation has been constructed by inserting and recovering artificial sources with known input size and magnitude into BoRG images. Source size is very helpful to help discriminate between high- and low-z sources, since direct measurements by Holwerda et al. (2015) on CANDELS galaxies show that $z > 9-10$ sources are more compact than $z \sim 2$ contaminants with similar colors. This empirical separation might be related to an approximate scaling of galaxy sizes as $(1+z)^n$ with $n \sim -1$ (Fall & Efstathiou 1980; Bouwens et al. 2004, 2006; Oesch et al. 2010), although a recent study by Curtis-Lake et al. (2016) highlights that the intrinsic sizes likely evolve less strongly with redshift ($n \sim -0.2$) compared to observed sizes. We discuss the contamination of our sample further in Section 5.1.

4.1. *borg_0240-1857_129*

This candidate is the brightest in the sample, with magnitude $H_{160} = 24.7$. It is robustly detected in H_{160} at S/N = 14.5, and marginally detected in J_{125} at S/N = 2.5, even though it is close to the edge of the chip. The source has a very red $J_{125} - H_{160}$ color, with $J_{125} - H_{160} = 2.2$. It also shows extended structure, and has $r_e = 0\farcs33$. Its photometric redshift solution is sharply peaked at $z = 10.1$, with a broad higher-redshift wing.

4.2. *borg_0240-1857_369*

This candidate, in the same field as the previous one is detected with magnitude $H_{160} = 25.2$, making it the second-brightest source in the sample. It is detected with S/N = 9.6 in H_{160}, and again marginally detected with S/N = 2.2 in J_{125}. It is the most extended source in the sample, with $r_e = 0\farcs38$. Its photometric redshift, like borg_0240-1857_129, is peaked at $z = 10.0$, with a broad higher-redshift wing.

4.3. *borg_0240-1857_25*

Field borg_0240-1857 includes a third bright candidate with $H_{160} = 26.4$, detected at S/N = 8.1. This source is not detected in the other bands (J_{125}, Y_{098} or V_{600}). Unlike the two brighter candidates, this object is more compact, with a measured half-light radius $r_e = 0\farcs13$. This is smaller than the PSF of the image ($0\farcs15$), indicating that it could be a point-source-like contaminant such as a cool dwarf star, although the stellarity of this source is 0.71, which is lower than the value expected for a point source (e.g. Schmidt et al. 2014 uses CLASS_STAR < 0.85 and Bouwens et al. 2015a CLASS_STAR < 0.9 to exclude stars).

This candidate is close to a foreground galaxy with $H_{160} = 26.0$, with a centre-to-centre projected separation of $1\farcs25$. While this foreground galaxy has an uncertain photometric redshift solution, it is likely to be at $z > 0.5$, based on its compact size. Using the framework developed by Barone-Nugent et al. (2015a) and Mason et al. (2015a), we estimate the gravitational lensing of this source. Magnification PDFs are obtained by estimating velocity dispersions from H_{160} magnitudes, using the empirical redshift-dependent Faber-Jackson relations given in Mason et al. (2015a) and Barone-Nugent et al. (2015a). Velocity dispersion is the best tracer of the strength of a strong gravitational lens (Turner et al. 1984; Schneider et al. 2006; Treu 2010). The Einstein radii of the foreground objects are modelled as singular isothermal spheres (e.g. Treu 2010) which depend on the velocity dispersion and the angular diameter distance to the source, and between the lens and source (where we use the best photo-z values). Assuming that the foreground source is at $z \sim 2$ (which maximizes lensing magnification), we infer a magnification $\mu = 1.1 \pm 0.1$.

4.4. *borg_0456-2203_1091*

This object has a magnitude $H_{160} = 26.1$ (S/N = 8.1), and is detected in the H_{160} only, with an extended but compact structure (effective radius $r_e = 0\farcs24$).

The source is located relatively close ($0\farcs5$ separation) to a hot pixel, which appears in the Y_{098} and J_{125} images. The H_{160}-band image is unaffected since it was acquired in a later orbit than the images in bluer bands. We carefully examined the individual FLT files and conclude that since the separation between the source center and the hot pixel is larger than twice r_e, and there is no sign of a hot pixel in the H_{160}-band, the identification of the candidate as a J_{125}-dropout is robust.

4.5. *borg_1153+0056_514*

This candidate is detected with a magnitude $H_{160} = 26.3$, and has S/N = 8.0. It is not detected in J_{125}, Y_{098} or V. It has an effective radius of $r_e = 0\farcs23$. This candidate is close to a foreground object ($1\farcs46$ centre-to-centre projected separation). The foreground object has an apparent magnitude $H_{160} = 25.0$, and is at an indeterminate photometric redshift. We use the same modelling framework as for borg_0240-1857_25 to estimate the lensing magnification of this source. Assuming that the source is at $z \sim 2$, we find a maximum $\mu = 1.2 \pm 0.1$.

Analysis of the FLT images of this field highlighted the presence of a bad pixel, correctly identified and masked by the data reduction pipeline, at the outer edge of the segmentation map of the dropout candidate in one of the two H_{160} frames. To determine the impact on the final photometry, we measured the source flux in the FLT frames separately, finding that the candidate is detected with S/N = 5.1 in the unaffected image and also S/N = 5.1 in the image affected by the bad pixel. Hence, we are confident that the source is real and that the photometry from the final drizzled image is robust.

4.6. *borg_1459+7146_785*

The sixth and final candidate is confidently detected at S/N= 12.8 in H_{160} ($H_{160} = 26.0$), and also in the J_{125} with S/N = 3.7. Its photometric redshift is sharply peaked at $z = 9.8$, with a secondary solution at $z \sim 2.5$. This candidate is also very compact, with measured half-light radius $r_e = 0\farcs14$, and the highest stellarity of the sample (CLASS_STAR = 0.91). Combining compactness

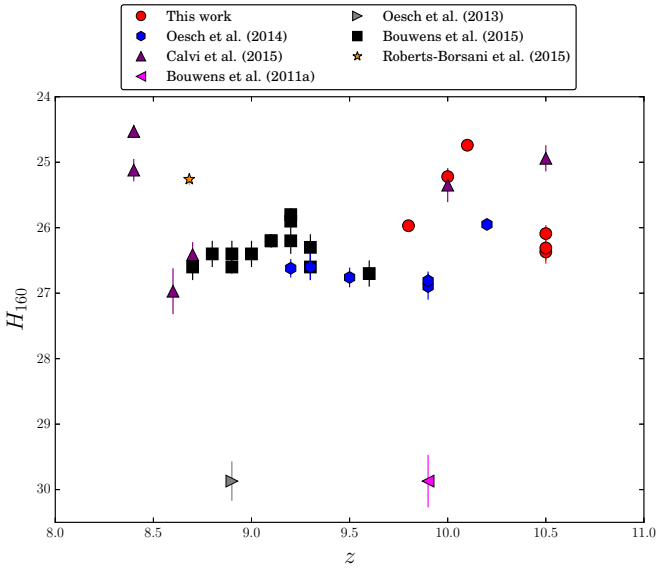

Figure 3. The apparent H_{160}-band magnitude vs. redshift for $z \geq 8$ galaxy candidates. The red circle points refer to the candidates described in Sections 4.1-4.6. Other points refer to candidates from other *HST*/WFC3 surveys as labelled. The redshift z is the photometric redshift for all candidates except that from Roberts-Borsani et al. (2015), where we use the spectroscopic redshift from Zitrin et al. (2015).

with high stellarity from a high S/N source, a stellar nature (cool dwarf) for this source is relatively likely, as we discuss in Section 5.1.

5. NUMBER DENSITY AND LUMINOSITY FUNCTION OF $z \sim 10$ GALAXIES

To translate the results on the search of possible candidates at $z \sim 10$ from the archival BoRG[z8] data into a number density/luminosity function determination, we need to assess both the impact of contamination in our sample, and the effective volume probed by the data.

5.1. *Contamination*

There are multiple classes of lower-z sources that may have similar $J_{125}-H_{160}$ colors to $z \sim 9-10$ Lyman-break galaxies (LBGs), such as Galactic stars, intermediate-redshift passive galaxies, and strong line emitters.

Cool, red stars in the Milky Way may be possible contaminants of our sample, although typical colors lack a strong $J_{125} - H_{160}$ drop. At low signal-to-noise ratio, the separation of point-like Galactic stars from resolved galaxies using the `SExtractor` CLASS_STAR parameter is not fully reliable. We use CLASS_STAR < 0.95 in our selection of J_{125}-dropouts in Section 3 to reject artifacts remaining from the reduction process, but this is not a strict enough criterion to reject all stars from our sample. In this case, five of our candidates identified as J_{125}-dropouts have CLASS_STAR < 0.8, with only borg_1459+7146_785 having CLASS_STAR > 0.9 (a value considered by Bouwens et al. 2015a as indicative of a stellar nature). Therefore we conclude that this source is most likely a stellar contaminant with unusual colors.

Emission-line galaxies are another source of contamination for $z \sim 9-10$ galaxy samples. For example, galaxies at $z \sim 3$ with strong [OII] emission may appear bright in H_{160}-band while the galaxy continuum is too faint to be detected in the other bands (Atek et al. 2011; Huang et al. 2015). Bouwens et al. (2015b) find that, at $z \sim 8$, the average density of extreme line emitters that enter the photometric selection is $\sim 10^{-3}$ per arcmin^{-2}, by creating mock catalogs of extreme emission line galaxies with varying J_{125} magnitude and spectral slope β. Extrapolating this result to $z \sim 10$, we expect to find $n_c = 0.3$ potential contaminants of this type over our survey area. This value is in line with previous spectroscopic observations of $z \sim 8$ BoRG candidates by Treu et al. (2012, 2013) using the MOSFIRE spectrograph on the Keck telescope, and by Barone-Nugent et al. (2015b) using XSHOOTER on the Very Large Telescope. These studies found no emission lines in the spectroscopy of $z \sim 8$ candidates, and are able to rule out emission lines from a low-z extreme emission line contaminant to 5σ, assuming that all of the H_{160} flux is due to a strong emission line. Barone-Nugent et al. (2015b) also find that, with a 3hr exposure, only a small part of the spectrum ($\sim 14\%$) is so affected by atmospheric transmission and absorption by OH lines that a strong emission line would not be detected to 2σ.

The last, and probably most severe class of contaminants, is that of passive and dusty galaxies that thus show a strong Balmer break and a very faint UV continuum. Under these conditions, $z \sim 2$ sources may mimic properties of LBGs and thus enter into our selection. Observations with *Spitzer*/IRAC at 3.6 and 4.5 μm can efficiently distinguish between high- and low-redshift sources. In fact, dusty $z \sim 2$ galaxies will appear 1-2 magnitudes brighter in [3.6] and [4.5] than in H_{160}, while $z \sim 9-10$ LBGs will have a relatively flat spectrum. Without Spitzer data, we rely on the size of the sources as proxy for the $H_{160} - [4.5]$ color, considering sources with $r_e > 0\farcs3$ as likely contaminants. Holwerda et al. (2015) find that, while the mean size of candidates in the $z \sim 10$ sample from Oesch et al. (2014) is $0\farcs13$, low-redshift, IRAC-red interlopers have a mean size of $0\farcs6$, but can be as small as $0\farcs35$, and there are no high-z candidates with sizes greater than $0\farcs2$ (Figure 4, Holwerda et al. 2015). Hence, we take $0\farcs3$ as a threshold. The two brightest sources in our sample are so extended to fall into such classification. The sources considered in Holwerda et al. (2015) are fainter than the $z \sim 10$ candidates in our sample, and so it is conceivable that the larger sizes of borg_0240-1857_129 and borg_0240-1857_369 are due to their higher luminosities. Using the size-luminosity relation derived in Holwerda et al. (2015), we infer that the size of a $z = 10$ galaxy at $M_{AB} = -22.7$ (the brightest in our sample) would be $0\farcs17 \pm 0\farcs04$, below our threshold of $0\farcs3$. This size cannot be used to completely reject extreme emission-line galaxies, which are likely to be more compact. For example, Huang et al. (2015) find that their sample of 52 extreme emission line galaxies in CLASH have FWHM $< 0\farcs9$, similar to our $r_e < 0\farcs3$ criterion for $z \sim 10$ candidates.

In addition to finding the redshift probability distribution of our six candidates using BPZ, we also fit SED templates described in Oesch et al. (2007). From this, we find an average probability $P(z < 8)$ of 54%. We conclude that three out of the six candidates, borg_1459+7146_785, borg_0240-1857_129, and borg_0240-1857_369, are likely to be contaminants. For the remaining three, contamination is still a possibility, and hence we make a conservative assumption of 33%

contamination (two out of three sources at $z \geq 10$), based on the estimate from the BoRG[z9-10] survey (Calvi et al. 2015) using the average probability $P(z < 8)$ for the candidates in their sample.

5.2. *Clustering in borg_0240-1857: evidence for or against contamination?*

Of the six possible candidates identified in the full BoRG[z8] survey, three of them, including the two brightest, are found in the same field (borg_0240-1857). The exposure time for this pointing is similar to the median of the survey ($t_{\rm exp} = 1400$ s in H_{160}), and thus such a catch is highly unlikely under the assumptions of a uniform distribution of candidates in the 62 fields analyzed here. Based on theoretical expectations, the presence of clustering can be used to verify the identity of bright high-z sources (Muñoz & Loeb 2008), under the broad assumption that UV luminosity is correlated with dark-matter halo mass (e.g., Trenti et al. 2010; Tacchella et al. 2013). Overdensities have also been identified at $z \sim 8$ in LBG samples (Trenti et al. 2012; Ishigaki et al. 2015b). However, one alternative possibility, more consistent with the relatively large size of the two bright J-dropouts, would be the presence of an overdensity of passive and dusty satellite galaxies within an intermediate redshift group. In either case, a further exploration of this configuration is very interesting since it can either identify an exciting overdensity of unexpectedly bright sources at $z \sim 10$, or shed light on the properties of intermediate redshift galaxies with extreme $J - H$ colors.

5.3. *Completeness*

We perform source recovery simulations to determine the efficiency and completeness of our selection, following Oesch et al. (2007, 2009, 2012). To do this, we insert and recover artificial galaxies with a Sérsic luminosity profile in the images. Half of the sources follow a de Vaucouleurs profile (Sérsic index $n = 4$), and the other half follow an exponential profile (Sérsic index $n = 1$), spanning a range of magnitudes ($24 \leq H_{160} \leq 28$), redshifts ($8.2 \leq z \leq 11.8$) and sizes (logarithmic distribution with mean $0\farcs175$ at $z \sim 7$, scaling as $(1+z)^{-1}$). The spectra of the sources are modeled as power law $f(\lambda) \propto \lambda^{\beta}$ with $\beta = -2.2 \pm 0.4$ (Gaussian distribution) with a sharp cutoff at rest-frame $\lambda = 1216$ Å. The intrinsic profiles of the artificial sources are convolved with the WFC3 PSF for each corresponding filter, before being inserted into the BoRG science images at random positions. Sources are then identified with `SExtractor`, and the statistics of the recovery rate is quantified. This is through the definition of $C(m)$ which is the completeness of the source detection, that is the probability of recovering an artificial source of magnitude m in the image, and of $S(z, m)$, which is the probability of identifying an artificial source of magnitude m and redshift z within the dropout sample, assuming that the source is detected. One example of the selection function for the dropout search in field borg_0440-5244 is shown in the bottom panel of Figure 4, while the upper panel of the same figure shows the overall effective volume probed by our search over all BoRG archival fields as a function of the apparent H_{160} magnitude.

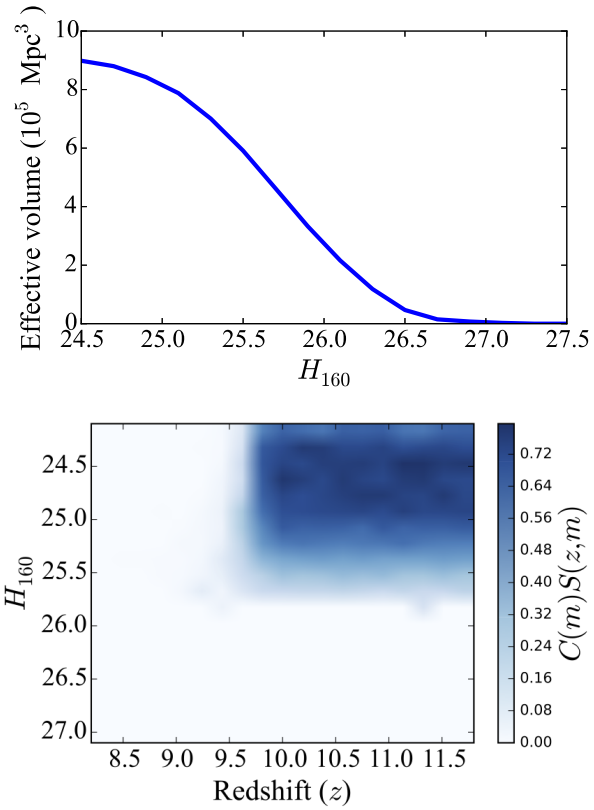

Figure 4. Top panel: The effective volume in comoving Mpc^3 recovered from simulations, as a function of the apparent H_{160} magnitude. Bottom panel: An example of the selection function $S(z, m)$ for field borg_0440-5244. The selection function is derived from simulations, by inserting and recovering artificial sources.

5.4. *Determination of the luminosity function*

From the discussion in Section 5.1, we consider the two brightest sources to be likely contaminants because of their large half-light radii, and we exclude the point-like source borg_1459+7146_785 as well. For the surviving three candidates we assume a contamination rate of 33%, e.g. we expect two sources to be at $z \sim 10$. After taking into account the effective volume probed by our selection, our estimates for the bright-end of the luminosity function at $z \sim 10$ is reported in Table 2, and shown in Figure 5. Interestingly, we infer a higher number density of bright sources than previous determinations by Bouwens et al. (2015a,b) around $M_{AB} \sim -21$, although the uncertainty is very large because of the small number of candidates. For brighter sources ($M_{AB} \lesssim -21.5$), our upper limits on $z \sim 10$ density are similar to those obtained in legacy fields, and strengthen the evidence for suppression of the abundance of galaxies at the bright-end of the luminosity function.

When compared to the initial results from the ongoing BoRG[z9-10] survey (Calvi et al. 2015), assuming that our two brightest sources are low-redshift contaminants, we do not find evidence of ultra-bright ($M_{AB} \sim -22$) galaxies despite analyzing data covering more than twice the area. If follow-up observations of our brightest sources indicate that they are likely at high redshift, we would instead determine that the LF is higher at the bright end than the upper limit from Bouwens et al. (2015a), and is instead consistent with the determina-

Table 2
Step-wise rest-frame UV LF at $z \sim 10$

$M_{UV,AB}$	$\phi\,(10^{-5}\,\mathrm{Mpc}^{-3}\,\mathrm{mag}^{-1})$
-22.78	< 0.26
-21.98	< 0.39
-21.18	$2.1^{+2.9}_{-1.4}$

tion by Calvi et al. (2015) at $M_{AB} = -22.3$.

Overall, our LF determination is higher, but still consistent at $\sim 2\sigma$ with the theoretical model of Mason et al. (2015b), shown as grey shaded area in Figure 5. Previous studies did not attempt unconstrained fits to the $z \sim 10$ LF, likely because of the small number of candidates. To evaluate the status of the situation with our additional datapoints, we attempt to derive Schechter parameters for a maximum likelihood fit to the stepwise LF data, carried out assuming a Poisson distribution for the number of galaxies expected in each bin (see Bradley et al. 2012). Due to the non-detection at $M_{\rm AB} = -19.23$ by Bouwens et al. (2015a), the LF is suppressed at the faint end. This leads to a likelihood landscape that is very flat over a wide region of the parameter space, and hence, we are unable to sufficiently constrain the Schechter parameters. Our fit attempt thus highlights that the dataset is still too small for tight quantitative constraints, but future growth in the number of candidates identified will allow rapid improvements.

Finally, we note that our conclusions rest on the assumption that the two brightest candidates we identified in field borg_0240-1857 are contaminants. If we were to include them in the analysis as $z \sim 10$ sources, we would infer that the LF would favor a power law at the bright end, rather than a Schechter form. Evidence for a single or double power-law form at high redshift has been seen in determinations of the LF at $z \sim 7-8$ (Bowler et al. 2014; Finkelstein et al. 2015, also earlier considered by Bouwens et al. 2011b), and potentially at $z \sim 10$ by Calvi et al. (2015), and may be naturally interpreted as a decrease in mass quenching from processes such as AGN feedback at high redshift (Bowler et al. 2014). Magnification bias, however, can also produce this effect on an otherwise Schechter-like LF. Thus, the astrophysical interpretation of our search ultimately rests on follow-up observations to establish the nature of the candidates borg_0240-1857_129 and borg_0240-1857_369. In any case, it is very interesting to note that the number of potential candidate J-dropouts that we identified is small (just six in over 60 fields), making further observations time-efficient, especially because half of the sources are clustered in a single pointing.

6. CONCLUSIONS

In this paper we presented a search for $z \sim 9-10$ candidates in archival data of the 2010-2014 Brightest of Reionizing Galaxies (BoRG[z8]) survey, a pure-parallel optical and near-infrared survey using *HST*/WFC3. While the survey was optimized to identify $z \sim 8$ sources as Y_{098}-dropouts, we searched over the deepest 293 arcmin^2 of the survey for J_{125}-dropout sources with $H_{160} \lesssim 26$, motivated by recent identification of very bright sources with $z \sim 9$. Our key results are:

- We identify six $z \sim 10$ galaxy candidates, detected in H_{160} at S/N > 8 and satisfying a conservative $J_{125} - H_{160}$ color selection with non-detection in bluer bands of the survey. The candidate's magnitudes vary from $H_{160} = 24.7$ to $H_{160} = 26.4$. Analysis of the surface brightness profile leads to the tentative identification of three contaminants, with the two brightest sources likely being intermediate redshift passive galaxies due to their size, and one faint source a galactic cool dwarf star because of the compact size and high stellarity.

- Of the six candidates, three are in the same field, borg_0240-1857, including the two brightest of the sample. Such strong clustering would be naturally explained if the sources were $z \sim 10$ (see Muñoz & Loeb 2008), despite contrary indication from r_e, but an alternative explanation of sub-halo clustering at intermediate redshift would also be viable.

- Based on our best estimate of the LF, we infer a higher galaxy number density for sources at $M_{AB} \sim -21$ compared to the observations of Bouwens et al. (2015a,b) and with the theoretical model of Mason et al. (2015b). However, our measurement is still consistent at the 2σ level with these studies.

- Irrespective of the nature of the two brightest sources in the sample, the selection criteria that we adopted yield a small number of candidates, very manageable for follow-up observations. This is quite remarkable, since the BoRG[z8] survey was not designed with $z \sim 10$ in mind, and the number of contaminants could have been much larger given the absence of a second detection band and the lack of a near-UV color to help remove passive and dusty intermediate redshift galaxies.

- Targeted follow-up observations can efficiently clarify the nature of the candidates we identified, help to further constrain the bright-end of the LF and characterize the properties of the yet unstudied population of compact intermediate redshift passive galaxies that mimic the colors of $z > 8$ sources.

The efficiency of targeted follow-ups and the overall potential to complement searches for $z \sim 10$ sources traditionally carried out in legacy fields are demonstrated by the very recent award of *Spitzer* IRAC time to our team to investigate the nature of the sources discussed here (PID #12058, PI Bouwens). With these observations, it will be possible to clarify the behavior of the bright end of the LF at $z \sim 10$, as well as to confirm ideal targets for further spectroscopic follow-up investigations without having to wait for *James Webb Space Telescope*.

SB, MT, and JW thank the Vatican Observatory, where part of this work was carried out, for kind hospitality. This work was partially supported by grants *HST*/GO 13767, 12905, and 12572. This research was conducted by the Australian Research Council Centre of Excellence for All-sky Astrophysics (CAASTRO), through project number CE110001020.

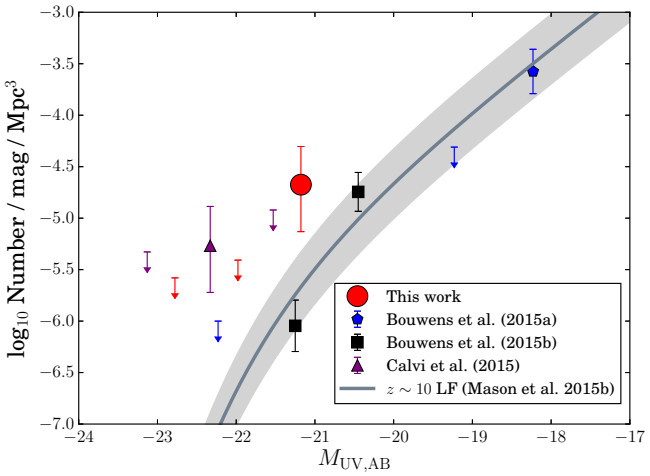
This work
Bouwens et al. (2015a)
Bouwens et al. (2015b)
Calvi et al. (2015)
$z \sim 10$ LF (Mason et al. 2015b)
$\log_{10}$ Number / mag / Mpc^3
$M_{\rm UV,AB}$

Figure 5. Step-wise determination of the UV LF at $z \sim 10$. The red circle and red upper limits refer to the values discussed in Section 5.4. Other symbols refer to Bouwens et al. (2015a,b); Calvi et al. (2015) as labelled. Error bars are 1σ Poisson errors, and limits are 1σ upper limits. Our best fit determination is shown as solid red line, while the dashed red line is one example of another equally acceptable fit, highlighting that the current data are insufficient for strong constraints on the LF shape. The overplotted gray line indicates the $z \sim 10$ LF from the theoretical model of Mason et al. (2015b), with shaded region being the 68% contour of its ϕ_* uncertainty.

REFERENCES

Alvarez, M. A., Finlator, K., Trenti, M. 2012, ApJ, 759, L38
Atek, H., Siana, B., Scarlata, C. et al. 2011, ApJ, 743, 121
Barone-Nugent, R. L., Trenti, M., Wyithe, J. S. B. et al. 2014, ApJ, 793, 17
Barone-Nugent, R. L., Wyithe, J. S. B., Trenti, M. et al. 2015a, MNRAS, 450, 1224
Barone-Nugent, R. L., Sonnenfeld, A., Wyithe, J. S. B. et al. 2015b, MNRAS, 453, 3068
Benítez, N., 2000, ApJ, 536, 571
Bertin, E. & Arnouts, S. 1996, A&AS, 117, 393-404
Bradley, L. D., Trenti, M., Oesch, P. A. et al. 2012, ApJ, 760, 108
Bouwens, R. J., Illingworth, G. D., Blakeslee, J. P., Broadhurst, T. J. & Franx, M. 2004, ApJ, 611, L1
Bouwens, R. J., Illingworth, G. D., Blakesless, J. P. & Franx, M. 2004, ApJ, 653, 53
Bouwens, R. J., Illingworth, G. D., Franx, M. & Ford, H. 2007, ApJ, 670, 928
Bouwens, R. J., Illingworth, G. D., Labbé, I. et al. 2011a, Nature, 469, 504
Bouwens. R. J., Illingworth, G. D., Oesch, P. A. et al. 2011b, ApJ, 737, 90
Bouwens, R. J., Bradley, L., Zitrin, A. et al. 2014, ApJ, 795, 126
Bouwens, R. J., Illingworth, G. D., Oesch, P. A. et al. 2015a, ApJ, 803, 34
Bouwens, R. J., Oesch, P. A., Labbé, I. et al. 2015b, arXiv:1506.01035v2
Bowler, R. A. A., Dunlop, J. S., McLure, R. J. et al. 2014, MNRAS, 440, 2810
Calvi, V., Trenti, M., Stiavelli, M. et al. 2015, arXiv:1512.05363
Caruana, J., Bunker, A. J., Wilkins, S. M. et al. 2012, MNRAS, 427, 3055
Casertano, S., de Mello, D., Dickinson, M. et al. 2000, AJ, 120, 2747
Coe, D., Zitrin, A., Carrasco, M. et al. 2013, ApJ, 762, 32
Curtis-Lake, E., McLure, R. J., Dunlop, J. S. et al. 2016, MNRAS, 457, 440
Ellis, R. S., McLure, R. J., Dunlop, J. S. et al. 2013, ApJ, 763, L7
Fall., S. M. & Efstathiou, G. 1980, MNRAS, 193, 189
Fialkov, A. & Loeb, A. 2015, ApJ, 806, 256
Finkelstein, S. L., Papovich, C., Dickinson, M. et al. 2013, Nature, 502, 524
Finkelstein, S. L., Ryan, R. E., Jr, Papovich, C. et al. 2015, ApJ, 810, 71
Giallongo, E., Menci, N., Castellano, M., Fontana, A., Grazian, A. & Pentericci, L. 2012, ApJ, 755, 124
Grazian, A., Fontana, A., Santini, P. et al. 2015, A&A, 575, A96
Grogin, N. A., Kocevski, D. D., Faber, S. M. et al. 2011, ApJS, 197, 35
Holwerda, B. W., Bouwens, R., Oesch, P., et al. 2015, ApJ, 808, 6
Huang, X., Zheng, W., Wang, J. et al. 2015, MNRAS, 801, 12
Illingworth, G. D., Magee, D., Oesch, P. A. et al. 2013, ApJS, 209, 6
Infante, L., Zheng, W., Laporte, N. et al. 2015, ApJ, 815, 18
Ishigaki, M., Kawamata, R., Ouchi, M., Oguri, M., Shimasaku, K., & Ono, Y. 2015, ApJ, 799, 12
Ishigaki, M., Ouchi, M. & Harikane, Y., 2015, arXiv150901751
Koekemoer, A. M., Fruchter, A. S., Hook, R. N. & Hack, W. 2003, in The 2002 HST Calibration Workshop: Hubble After the Installation of the ACS and the NICMOS Cooling System, ed. S. Arribas, A. Koekemoer, & B. Whitmore (Baltimore, MD: STScI), 337
Koekemoer, A. M., Faber, S. M., Ferguson, H. C. et al. 2011, ApJS, 197, 36
Labbé, I., González, V., Bouwens, R. J. et al. 2010, ApJ, 716, L103
Labbé, I., Oesch, P. A., Illingworth, G. D. et al. 2015, arXiv:1507.08313
Madau, P., Haardt, F., & Rees, M. J. 1999, ApJ, 514, 648
Madau, P. & Haardt, F. 2015, ApJ, 813, L8
Malhotra, A., Rhoads, J. E., Pirzkal, N. et al. 2005, ApJ, 626, 666
Mason, C. A., Treu, T., Schmidt, K. B. et al. 2015a, ApJ, 805, 79
Mason, C. A., Trenti, M. & Treu, T. 2015b, ApJ, 813, 21
McLeod, D. J., McLure, R. J., Dunlop, J. S., Robertson, B. E., Ellis, R. S., & Targett, T. A. 2015, MNRAS, 450, 3032
McLure, R. J., Dunlop, J. S., Bowler, R. A. A. et al. 2013, MNRAS, 432, 2696
Muñoz, J. A. & Loeb, A. 2008, MNRAS, 385, 2175
Muñoz, J. A. & Loeb, A. 2011, ApJ, 729, 99
Oesch, P. A., Stiavelli, M., Carollo, C. M. et al. 2007, ApJ, 671,1212
Oesch, P. A., Carollo, C. M., Stiavelli, M. et al. 2009, ApJ, 690, 1350
Oesch, P. A., Bouwens, R. J., Carollo, C. M. et al. 2010, ApJ, 709, L21
Oesch, P. A., Bouwens, R. J., Illingworth, G. D. et al. 2012, ApJ, 759, 135
Oesch, P. A., Bouwens, R. J., Illingworth, G. D. et al. 2013, ApJ, 773, 75
Oesch, P. A., Bouwens, R. J., Illingworth, G. D. et al. 2014, ApJ, 786, 108
Oesch, P. A., van Dokkum, P. G., Illingworth, G. D. et al. 2015, ApJ, 804, L30
Oke, J. B. & Gunn, J. E. 1983, ApJ, 266, 713
Pentericci, L., Fontana, A., Vanzella, E. et al. 2011, ApJ, 743, 132
Pentericci, L., Vanzella, E., Fontana, A. et al. 2014, ApJ, 793, 113
Planck Collaboration, Ade, P. A. R., Aghanim, N. et al. 2015, arXiv:1502.01589
Postman, M., Coe, D., Bénitez, N. et al. 2012, ApJS, 199, 25
Roberts-Borsani, G. W., Bouwens, R. J., Oesch, P. A. et al. 2015, arXiv:1506.00854
Schechter, P. 1976, ApJ, 203, 297
Schenker, M. A., Stark, D. P., Ellis, R. S. et al. 2012, ApJ, 744, 179
Schlafly, E. F., Finkbeiner, D. P. 2011, ApJ, 737, 103
Schmidt, K. B., Treu, T., Trenti, M. et al. 2014, ApJ, 786, 57
Schneider, P., Kochanek, C. S. & Wambsganss, J. 2006, Gravitational Lensing: Strong, Weak and Micro (Berlin: Springer)
Stark, D. P., Ellis, R. S., Bunker, A. et al. 2009, ApJ, 697, 1493
Stark, D. P., Ellis, R. S., Chiu, K., Ouchi, M. & Bunker, A. 2010, MNRAS, 408, 1628
Stark, D. P., Richard, J., Charlot, S. et al. 2015, MNRAS, 450, 1846
Stark, D. P., Walth, G., Charlot, S. et al. 2015, MNRAS, 454, 1393
Steidel, C. C., Giavalisco, M., Pettini, M., Dickinson, M., & Adelberger, K. L. 1996, ApJ, 462, L17
Tacchella, S., Trenti, M. & Carollo, C. M. ApJ, 768, L37

Tilvi, V., Papovich, C., Finkelstein, S. L. et al. 2014, ApJ, 794, 5
Trenti, M. & Stiavelli, M. 2008, ApJ, 676, 767
Trenti, M., Stiavelli, M., Bouwens, R. J. et al. 2010, ApJ, 714, L202
Trenti, M., Bradley, L. D., Stiavelli, M. et al. 2011, ApJ, 727, L39
Trenti, M., Bradley, L. D., Stiavelli, M. et al. 2012, ApJ, 746, 55
Treu, T. 2010, ARA&A, 48, 87
Treu, T., Trenti, M., Stiavelli, M., Auger, M. W. & Bradley, L. D. 2012, ApJ, 747, 27
Treu, T., Schmidt, K. B., Trenti, M., Bradley, L. D., & Stiavelli, M. 2013, ApJ, 775, L29
Turner, E. L., Ostriker, J. P.
van Dokkum, P. G. 2001, PASP, 113, 1420
Vanzella, E., Fontana, A., Pentericci, L. et al. 2014, A&A, 569, A78
Willott, C. J., Delorme, P., Omont, A. et al. 2007, AJ, 134, 2435
Wyithe, J. S. B., Yan, H., Windhorst, R. & Mao, S. 2011, Nature, 469, 181
Yan, H., Yan, L., Zamojski, M. A. et al. 2011, ApJ, 728, L22
Zheng, W., Postman, M., Zitrin, A. et al. 2012, Nature, 489, 406
Zheng, W., Shu, X., Moustakas, J. et al. 2014, ApJ, 795, 93
Zitrin, A., Zheng, W., Broadhurst, T. et al. 2014, ApJ, 793, L12
Zitrin, A., Labbé, I., Belli, S. et al. 2015, arXiv:1507.02679